CMS Physics Analysis Summary

Contact: cms-pag-conveners-fsq@cern.ch 2014/03/22

Measurement of double differential Drell-Yan and associated jet cross sections at low and high invariant masses in proton-proton collisions at $\sqrt{s} = 7$ TeV

The CMS Collaboration

Abstract

Measurements of the differential Drell-Yan and associated jet cross section as a function of the Drell-Yan pair mass are presented in the di-muon channel. The data set is based on an integrated luminosity of 4.9 fb^{-1} of proton-proton collision data recorded with the CMS detector at the LHC at $\sqrt{s} = 7$ TeV. Cross sections as a function of the Drell-Yan di-muon transverse momentum are measured differentially in the di-muon mass range of 30 to 1500 GeV. The cross section for Drell-Yan production in association with one or two jets with $p_{\mathrm{T}}^{\mathrm{jet}} > 30$ GeV in the range $|\eta^{\mathrm{jet}}| < 4.5$ is measured. In addition, the jet multiplicity in Drell-Yan production as a function of the rapidity separation of the leading jet and the Drell-Yan pair is presented. All measurements are compared to predictions of MADGRAPH+PYTHIA6 Monte Carlo event generator based on multiparton matrix elements plus parton showers.

1 Introduction

The production of Drell-Yan (DY) lepton pairs in hadron-hadron collisions is described as an s-channel γ^*/Z exchange at leading order (LO). Theoretical calculations for inclusive DY lepton pair production as a function of the DY lepton pair mass and transverse momentum p_{T} are available up to next-to-next-to-leading order (NNLO) in perturbative quantum chromodynamics (pQCD) [1–4]. While DY lepton pair production at large transverse momenta can be described with fixed leading or next-to-leading order calculations in pQCD, the description at small p_{T} requires resummation of soft gluons to all orders in perturbation theory [5, 6]. The p_{T} distribution of DY lepton pairs has been measured at LHC energies in the Z mass range [7], but the corresponding measurements as a function of the DY lepton pair mass m_{DY} are not available.

Of special interest is the p_{T} spectrum of the DY lepton pair and the contribution from non-perturbative and perturbative multi-gluon resummation. In inclusive DY lepton pair production, the resummation effects are concentrated at small p_{T} with the maximum of the p_{T} distribution being around 5 GeV, not depending much on the DY lepton pair mass. If however a jet with large p_{T} is required in addition, the p_{T} spectrum of DY lepton pair is shifted towards larger transverse momenta, thus allowing to study multiple-gluon emission and resummation effects in the perturbative region and to separate them from the non-perturbative contribution at small p_{T}.

Multi-jet emissions in a pseudorapidity interval between the DY lepton pair and a leading jet are a sensitive probe for multi-gluon emissions [8]. At large rapidity separation between the DY lepton pair and the jet, a fixed order approach is expected to fail, and again perturbative multi-jet resummation might play a significant role. Of additional interest is the jet multiplicity between the DY lepton pair and the leading jet, as resummation might lead to a different behavior compared to a fixed order prediction. The detailed measurements of inclusive DY lepton pair production as well as DY lepton pair production in association with jets, especially in the mass range above the Z mass (and in the range of $m_{\mathrm{DY}} \sim 125$ GeV), is important for a later comparison with Higgs production, which can be used to determine the differences of soft gluon and multi-jet resummation in a quark or gluon induced process [9].

In this paper a measurement of the differential Drell-Yan and associated jet cross section for various ranges of Drell-Yan di–muon mass m_{DY} using an integrated luminosity of 4.9 fb^{-1} in the di-muon channel of proton-proton collision data recorded with the CMS detector at the LHC at $\sqrt{s} = 7$ TeV is presented. Differential cross sections as a function of the Drell-Yan di–muon transverse momentum are measured differentially in the di–muon mass range of $30 < m_{\mathrm{DY}} < 1500$ GeV. The cross sections for Drell-Yan production in association with at least one or two jets (in the following DY + 1 jet and DY + 2 jets, respectively) with $p_{\mathrm{T}}^{\mathrm{jet}} > 30$ GeV in the range $|\eta^{\mathrm{jet}}| < 4.5$ are measured, where $\eta = -\ln[\tan(\theta/2)]$ and θ is the polar angle with respect to the anti-clockwise beam direction. Jets are reconstructed by the anti-k_{T} algorithm [10–12] with a radius parameter of 0.5. In addition the jet multiplicity in Drell-Yan production as a function of the separation in rapidity between the leading jet and the Drell-Yan muon pair is presented.

2 The CMS detector

The central feature of the Compact Muon Solenoid (CMS) apparatus is a superconducting solenoid of 6 m internal diameter, providing a magnetic field of 3.8 T. Within the superconducting solenoid volume are a silicon pixel and strip tracker, a lead tungstate crystal electro-

magnetic calorimeter (ECAL), and a brass/scintillator hadron calorimeter (HCAL). Muons are measured in gas-ionization detectors embedded in the steel return yoke outside the solenoid. Extensive forward calorimetry complements the coverage provided by the barrel and endcap detectors.

CMS uses a right-handed coordinate system, with the origin at the nominal interaction point, the x axis pointing to the centre of the LHC, the y axis pointing up (perpendicular to the LHC plane), and the z axis along the anticlockwise-beam direction. The polar angle θ is measured from the positive z axis and the azimuthal angle ϕ is measured in the x-y plane.

The particle-flow event reconstruction consists in reconstructing and identifying each single particle with an optimised combination of all subdetector information. The energy of photons is directly obtained from the ECAL measurement, corrected for zero-suppression effects. The energy of electrons is determined from a combination of the track momentum at the main interaction vertex, the corresponding ECAL cluster energy, and the energy sum of all bremsstrahlung photons attached to the track. The energy of muons is obtained from the corresponding track momentum. Muons are measured in the pseudorapidity range $|\eta| < 2.4$, with detection planes made using three technologies: drift tubes, cathode strip chambers, and resistive plate chambers. Matching muons to tracks measured in the silicon tracker results in a relative transverse momentum resolution for muons with $20 < p_{\mathrm{T}} < 100\,\mathrm{GeV}$ of 1.3–2.0% in the barrel and better than 6% in the endcaps. The p_{T} resolution in the barrel is better than 10% for muons with p_{T} up to 1 TeV [13]. The energy of charged hadrons is determined from a combination of the track momentum and the corresponding ECAL and HCAL energy, corrected for zero-suppression effects, and calibrated for the nonlinear response of the calorimeters. Finally the energy of neutral hadrons is obtained from the corresponding calibrated ECAL and HCAL energy.

For each event, hadronic jets are clustered from these reconstructed particles with the infrared and collinear safe anti-k_{T} algorithm, operated with a size parameter R of 0.5. The jet momentum is determined as the vectorial sum of all particle momenta in this jet, and is found in the simulation to be within 5% to 10% of the true momentum over the whole p_{T} spectrum and detector acceptance. An offset correction is applied to take into account the extra energy clustered in jets due to additional proton-proton interactions within the same bunch crossing. Jet energy corrections are derived from the simulation, and are confirmed with in situ measurements with the energy balance of dijet and photon+jet events [14]. Additional selection criteria are applied to each event to remove spurious jet-like features originating from isolated noise patterns in certain HCAL regions. The jet energy resolution amounts typically to 15% at 10 GeV and 8% at 100 GeV to be compared to about 40% and 12%, obtained when the calorimeters alone are used for jet clustering.

A more detailed description can be found in Ref. [15].

3 Data and Monte Carlo samples

The measurements presented in this paper are based on pp collision data recorded in 2011 with the CMS detector at the LHC at $\sqrt{s} = 7$ TeV, corresponding to an integrated luminosity of 4.9 fb^{-1}.

The determination of efficiencies and backgrounds from processes that result in two muons as well as the determination of systematic uncertainties is performed using Monte Carlo (MC) event samples. Control samples of data are used to determine muon reconstruction efficien-

cies, to validate the efficiencies and background processes determined by the MC samples. The MC samples are produced by the MADGRAPH [16] (version 5) and PYTHIA [17] (version 6.4.33) event generators. These samples are passed through the full CMS detector simulation based on GEANT4 [18] which includes trigger simulations and the full chain of the CMS event reconstruction.

The Drell-Yan signal samples are generated with the MADGRAPH generator which generates $N \leq 4$ partons in the final state. Electroweak production of the Drell-Yan lepton pair is not included in the MADGRAPH MC predictions. The background contributions from $Z \to \tau\tau$, $t\bar{t}$ and W+jets production are also generated with MADGRAPH. For cross check of the unfolding an event sample generated with POWHEG [19] for inclusive DY production is used. All samples are interfaced with PYTHIA to simulate the parton shower, hadronisation and underlying event. In all cases the tune Z2 (tune Z2 is identical to tune Z1 described in [20] except that Z2 employs the CTEQ6L [21] parton distribution function while Z1 uses CTEQ5L) is used to simulate the underlying event. The backgrounds from dibosons (WW, WZ, ZZ) and QCD multi-jets are produced with PYTHIA Z2.

4 Cross section measurements

In this analysis the differential cross sections of the DY di-muon pair as well as associated jets as a function of the DY di-muon mass m_{DY} are measured. The measured spectra are corrected for efficiency and detector acceptance effects. The measured cross sections are obtained from

$$\sigma = \frac{N}{\rho\,\mathcal{L}_{\mathrm{int}}}, \tag{1}$$

where N denotes the signal yield, defined as the number of background subtracted events, corrected for efficiency and detector effects. The scale factor ρ accounts for the differences in simulation and data efficiencies and $\mathcal{L}_{\mathrm{int}}$ is the total integrated luminosity. In order to account for bin-migrations the cross section is unfolded and corrected for detector effects.

The measurement is performed for a pair of muons with $|\eta^{\mu}| < 2.1$ and $p_{\mathrm{T}}^{\mathrm{lead}\,\mu} > 20$ GeV and $p_{\mathrm{T}}^{\mathrm{sublead}\,\mu} > 10$ GeV and a Drell-Yan di–muon mass $30 < m_{\mathrm{DY}} < 1500$ GeV. Jets are required to have $p_{\mathrm{T}}^{jet} > 30$ GeV with $|\eta^{jet}| < 4.5$. No extrapolation to the total cross section is performed.

The cross section in the Z peak region ($60 < m_{\mathrm{DY}} < 120$ GeV) integrated over the dimuon p_{T}, σ_{Z}, is used to normalize all cross sections for the three different topologies (inclusive, DY + 1 , DY + 2 jet) to reduce systematic uncertainties.

4.1 Primary vertex reconstruction

To reconstruct the primary vertices from the tracks of the particles, the Deterministic Annealing clustering method [22] is used. A selected vertex can be defined as a primary vertex if the z position of the vertex is within 24 cm of the nominal detector centre and the radial position within 2 cm from the beam spot. From this set of selected primary vertices the hard interaction vertex is selected as the vertex with the maximum sum of the transverse momenta of the tracks associated with this vertex. The muons and the jets are required to emerge from the primary vertex.
In order to suppress the contamination from $\gamma\gamma \to \mu^{+}\mu^{-}$ events a minimum cut on the number of tracks associated with the primary vertex is set to three.

At high luminosities several pp interactions can happen simultaneously (pileup). In order to reproduce the number of pileup interactions observed in data, a weight factor is applied to the simulation based on the instantaneous luminosity and the total inelastic cross section, for which an uncertainty of 5% on the inelastic cross section is taken into account.

4.2 Muon selection

Events with muons are triggered by muon candidates within $|\eta^{\text{lead}\,\mu}| < 2.1$ and $|\eta^{\text{sublead}\,\mu}| < 2.4$ with $p_{\text{T}}^{\text{lead}\,\mu} > 20$ GeV and $p_{\text{T}}^{\text{sublead}\,\mu} > 10$ GeV. Muon candidates are reconstructed with the particle–flow (PF) algorithm [23, 24] which is based on the tracker and the muon system. Muon candidates must pass the standard CMS muon identification and quality control criteria, which are based on the number of hits found in the tracker, the response of the muon detector and a set of matching criteria between the parameters measured by the CMS tracker and those from the muon detector. Two oppositely charged muons are selected if they fulfill the following preselection selection criteria. The two muons have to be isolated to ensure they are originating from an electroweak process. The isolation criterion is based on the PF based relative isolation variable defined as

$$\text{Iso}_{\mu}^{\text{PF}} = \frac{\sum \left(p_{\text{T}}^{\text{charged}} + p_{\text{T}}^{\gamma} + p_{\text{T}}^{\text{neutral}} \right)}{p_{\text{T}}^{\mu}}. \tag{2}$$

The sum runs over all charged particles emerging from the hard interaction vertex. Only particles within a cone of $\Delta R < 0.4$ around the muon momentum are selected. The sum of the transverse momentum of the neutral hadrons and photons is corrected for additional activity from pileup, by using the $\Delta\rho$ correction. ρ is defined as the energy density in the η–ϕ plane from pileup and underlying event. The muon isolation variable is required to be less than 0.1 (0.15) for muons with p_{T} greater (smaller) than 20 GeV.

4.3 Jet selection

The jets are reconstructed from measured PF objects by the anti-k_{T} clustering algorithm using the parameter $R = 0.5$. Jets are clustered excluding the decay products of the Drell-Yan process. In all cases the jets must have $p_{\text{T}} > 30$ GeV and $|\eta^{\text{jet}}| < 4.5$. In the following the kinematic selection criteria for the muons and the jets are referred to as preselection. The jets must be separated from the two muons in the final state by $\Delta R > 0.5$. The jets require the loose PF jet identification. In addition, various criteria are applied to identify jets coming from pileup [25].

4.4 Background estimation

There are several background processes which contribute to the di-muon final state. In the Z peak region (60–120 GeV) the signal is nearly background free and the dominant contribution is Z boson exchange. In the low mass region (30–60 GeV) the main background contributions are due to multi-jet QCD events and the Z decaying into τ pairs. Beyond the Z mass (120–1500 GeV) the dominant sources of additional di-muon production are $t\bar{t}$ and di-boson processes.

The estimation on the QCD background is obtained by a data-driven method using same-sign (SS) dimuon events. The number of opposite-sign (OS) QCD events after isolation cut in the signal region can then be estimated by

$$N_{\mathrm{QCD}}^{\mathrm{OS}} = N_{\mathrm{QCD}}^{\mathrm{SS}} R_{\mathrm{QCD}}\,(\mathrm{OS/SS})\,, \tag{3}$$

where $N_{\mathrm{QCD}}^{\mathrm{SS}}$ gives the number of QCD events in the SS data sample with the same selection criteria as for the OS sample. The ratio $R_{\mathrm{QCD}}\,(\mathrm{OS/SS})$ of OS over SS events cannot be evaluated precisely applying the isolation cut on the SS sample, because it removes most of the events. Therefore the ratio is evaluated in the SS data sample with orthogonal selection criteria to the net charge of the muon pair. It has been found that ratio with direct or inverse isolation cut are the same. In addition the muon net charge plays no role, and therefore the inverted isolation cut of $\mathrm{Iso}_{\mu_{1,2}} > 0.5$ can be used. An uncertainty of 100% is assigned to the background estimation.

For the top pair background the MC is scaled to describe the region with $E_{\mathrm{T}}^{\mathrm{miss}} > 80$ GeV. The resulting normalization is consistent with the approximate NNLO calculation [26, 27] as well as with the CMS measurement [28]. A 10% uncertainty in the scale factor is assigned. In order to reduce the top pair background contribution a cut on the missing transverse energy is applied, $E_{\mathrm{T}}^{\mathrm{miss}} > 80$ GeV. It has been verified with simulation that the shape of the distributions in the region $E_{\mathrm{T}}^{\mathrm{miss}} < 80$ GeV describes the measurement.

The yields of di-boson production (WW, WZ and ZZ) are scaled to the cross sections predicted by theory in NLO [4, 29]. An uncertainty of 30% on the normalization is assigned. The contribution from single W production is normalized to the inclusive cross section as measured by CMS [30]. The uncertainty is derived by limited MC statistics of selected W+jet events and amounts to 25–50% but has no visible effect on the analysis results.

The shapes of $Z \to \tau\tau$ background is estimated with MADGRAPH MC predictions and it is normalized to Z+jets cross-section measured by CMS. An uncertainty of 3% is assigned to the normalization.

4.5 Correction to stable particle level

Several correction methods are applied to the data to obtain the jet cross section at the stable particle level (decay length $c\tau > 10$mm).

The observed number of events has to be corrected for detector resolution effects. In order to estimate the migration effects from hadron to detector level, two quantities are defined. The bin purity is defined as the fraction of events on detector level that stay in this bin when going to hadron level and the stability of the bin describes how many events remain in this bin when going from hadron to detector level. For $p_{\mathrm{T}}^{\mu\mu} < 20$ GeV the purity is around 60–80% while for $p_{\mathrm{T}}^{\mu\mu} > 20$ GeV it increases to 90 % due to increased bin size. This behavior is similar for all invariant mass bins, and for DY + 1 jet and DY + 2 jet production. The off-diagonal elements of the normalized response matrix for the transverse momentum for inclusive Drell-Yan production are smaller than 10% for the neighboring bins, indicating small migration effects. For the differential cross section as a function of $|\Delta y(\mu\mu, \mathrm{j}_1)|$ the purity and stability is $> 90\%$ for the different mass bins.

The Bayes unfolding method [31] is used for the unfolding. Jets coming from pileup interactions as well as effects due to jet p_{T} migrations into the fiducial region are taken into account by the unfolding procedure. It is assumed that MADGRAPH models correctly the migrations into and out of the phase space. The migration effect in and out of the fiducial region is of the order of 30 % at low dimuon p_{T}. For $p_{\mathrm{T}} > 40$ GeV the migration effects are $< 20\%$. In order to estimate an uncertainty on the unfolding a different MC generator is used to determine the response matrix. To gain a dependence on the physics model the POWHEG generator is used.

POWHEG generates the hard matrix element of DY + 1 jet at NLO and is interfaced with PYTHIA to model the parton shower. POWHEG predictions are not able to describe the jet variables with jet multiplicity larger than one. Therefore the comparison in the unfolding is done by selecting DY + exactly one jet. Due to large contributions from background events at low dimuon p_T the POWHEG sample is reweighted to describe the data. The uncertainty is then estimated by using a sample of POWHEG and MADGRAPH events to determine the response matrix.

Further corrections like event efficiencies, which are defined as the fraction of events passing the reconstruction and selection cuts within the fiducial region, are considered. The trigger, muon identification and selection efficiencies are obtained from $Z \to \mu^+\mu^-$ events from data and MC samples using the tag-and-probe method [30].

The MC events are corrected for trigger, muon identification and isolation efficiencies. To compensate for differences in data and MC efficiencies scale factors , which are defined as the ratio of the efficiencies in data and MC, are applied to the MC events.

The leptons in the final state of the Drell-Yan process can radiate nearly collinear photons. This effect is referred to as QED final-state radiation (QED FSR). The cross sections in this paper correspond to particle level results, which corresponds to bare muons. Bare muons are defined after the QED FSR.

4.6 Systematic uncertainties

The measurement of the Drell-Yan $p_T^{\mu\mu}$ and the rapidity separation between the forward Drell-Yan pair and the leading jet is performed in bins of the dimuon mass in the range 30–1500 GeV. Systematic uncertainties due to luminosity, pileup and QED FSR effects cancel out or are negligible when normalized to the cross section in the Z boson mass region (60–120 GeV).
For all uncertainty sources the effect directly translates into an uncertainty in the cross section measurement. The systematic uncertainties are summarized in Tab. 1 and Tab. 2.

The main sources of systematic uncertainties affecting the Drell-Yan and Drell-Yan +jet cross section measurement are:

- Unfolding
  Only small migrations between neighboring bins are observed. The MADGRAPH MC samples reproduce well the measured data and thus is sufficient for the correction. As a cross check, the response matrix obtained from the POWHEG sample is also used and the difference between the results obtained using MADGRAPH and POWHEG is taken as a systematic uncertainty.
- Jet energy calibration (JEC)
  An uncertainty between 3–5% on the jet energy scale is assigned depending on the transverse momentum and the pseudorapidity of the jet [32, 33]. The final distributions are compared by varying the JEC up and down within its uncertainty. The JEC uncertainty is the dominant uncertainty source in the distributions including jets.
- Pileup reweighting procedure
  The uncertainty on the pileup modeling of the simulated events is estimated according to the distribution of the number of interactions per beam crossing. The uncertainty is obtained from the total inelastic cross section varied by $\pm 5\%$ around the nominal value of 68 mb, based on a set of models consistent with the cross section measured by the CMS experiment [34].
- Efficiency correction
  A statistical and systematic uncertainty from the Tag and Probe method on the trig-

ger efficiency and muon isolation and identification scale factors are assigned. The uncertainty is estimated to be 2%. The extrapolation of scale factors from low to high p_T uses the total scale factor calculated at low p_T, adding a systematic uncertainty of the order of 2–3% for the extrapolation to high p_T.

- Background estimation
  The final results show the background-subtracted yield. Therefore an uncertainty in the estimation of the background process is assigned. Furthermore an uncertainty due to the limited number of simulated events has to be assigned. The number of background events is varied by $\pm\sqrt{N}$ and the uncertainty of the normalization and background estimation is taken into account.

Table 1: Summary of typical systematic uncertainties of the Drell-Yan di-muon transverse momentum in different bins of the di-muon mass. The total systematic uncertainties are given by the quadratic sum of each individual sources. The first values are for inclusive Drell-Yan production, the second ones for DY + 1 jet and the third ones for DY + 2 jet production

$m^{\mu\mu}$ bin (GeV)	Unfolding (%)			JEC (%)			PU (%)			Eff. (%)			Bkg Est. (%)		
30 - 45	10	8	8	-	10	15	4	5	6	4	4	4	2	3	4
45 - 60	3	10	10	-	10	10	2	2	3	4	4	4	2	2	5
60 - 120	2	2	2	-	8	10	2	2	2	4	4	4	1	1	1
120 - 200	5	5	5	-	8	10	2	2	2	4	4	4	3	4	10
200 - 1500	10	15	15	-	10	10	3	4	4	8	8	8	6	5	15

Table 2: Summary of typical systematic uncertainties of $|\Delta y(\mu\mu, \mathrm{j}_1)|$ distribution in DY + 1 jet (DY + 2 jets) events in different bins of the di-muon mass. The total systematic uncertainties are given by the quadratic sum of each individual sources.

$m^{\mu\mu}$ bin (GeV)	Unfolding (%)		JEC (%)		PU (%)		Eff. (%)		Bkg Est. (%)	
30 - 60	10	10	15	10	5	6	4	4	3	1
60 - 120	8	8	8	9	2	2	4	4	1	1
120 - 1500	15	15	10	8	5	8	4	4	1	2

5 Results

The cross sections for inclusive Drell-Yan production, as well as for DY + 1 jet and DY + 2 jet production are given below, unfolded to stable particle level for Drell-Yan production in the phase space defined by $p_T^{\mathrm{lead}\mu} > 20$ GeV, $p_T^{\mathrm{sublead}\mu} > 10$ GeV and $|\eta^\mu| < 2.1$. Jets are reconstructed with the anti-k_T algorithm using $R = 0.5$ with $|\eta| < 4.5$ and $p_T > 30$ GeV. The cross sections presented are normalized to the cross section in the Z peak region (60–120 GeV). In all distributions the data points are shown at the center of the bin and no bin-center correction is applied.

5.1 Inclusive Drell-Yan double differential Cross Section $\mathrm{d}^2\sigma/\mathrm{d}m^{\mu\mu}\mathrm{d}p_T^{\mu\mu}$

The double differential cross section for inclusive DY lepton pair production as a function of $m^{\mu\mu}$ and $p_T^{\mu\mu}$ is shown in Fig. 1, the cross section for the inclusive DY + 1 jet production is shown in Fig. 2, and the cross section for the inclusive DY + 2 jets production is shown in Fig. 3.

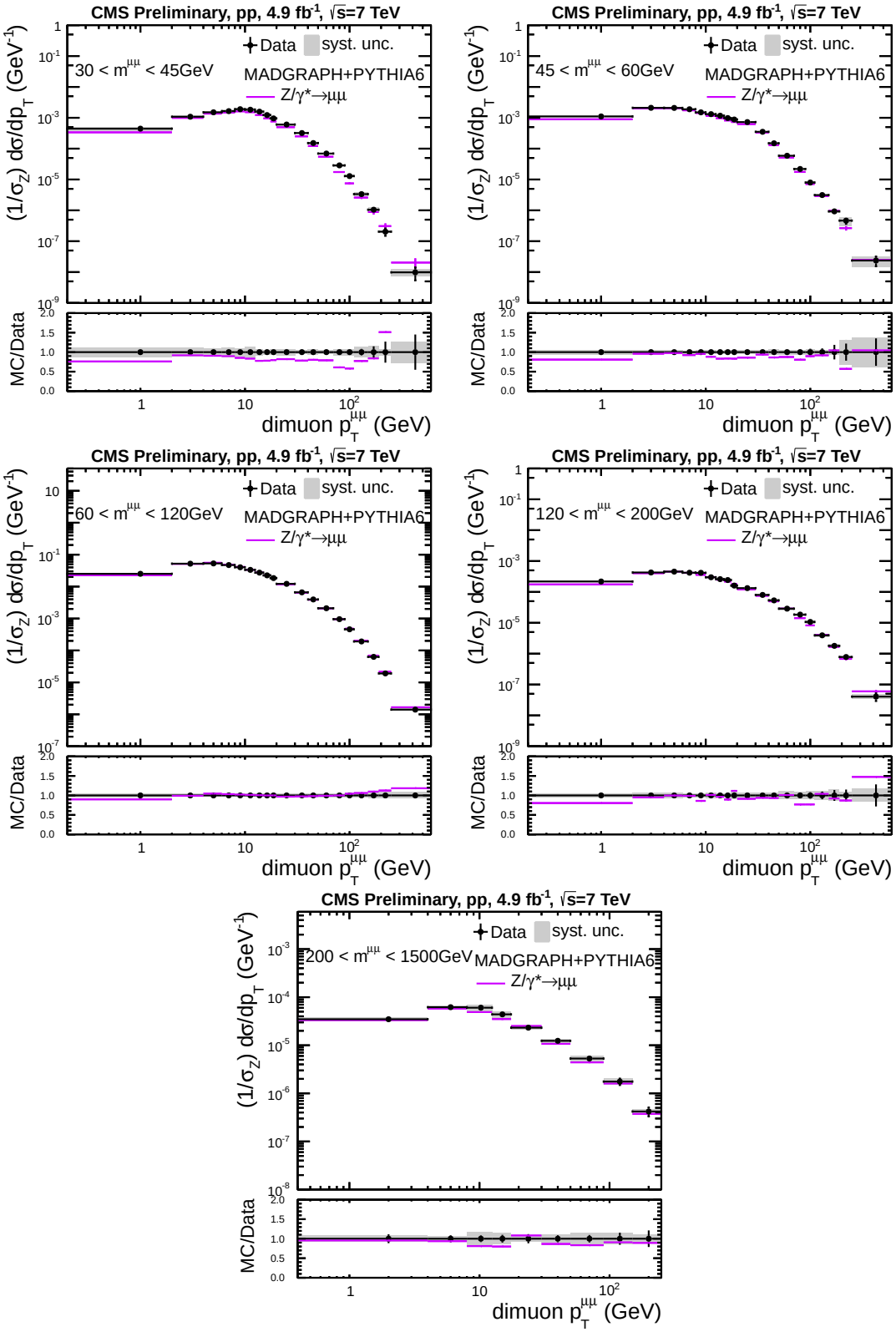

Figure 1: Drell-Yan di-muon transverse momentum distribution normalized to the Z resonance region (60–120 GeV) in five different invariant mass regions covering the range from 30 – 1500 GeV. The vertical error bars on data indicate the statistical uncertainties and the error band represents the correlated systematic uncertainties. Data are compared to MADGRAPH + PYTHIA 6.

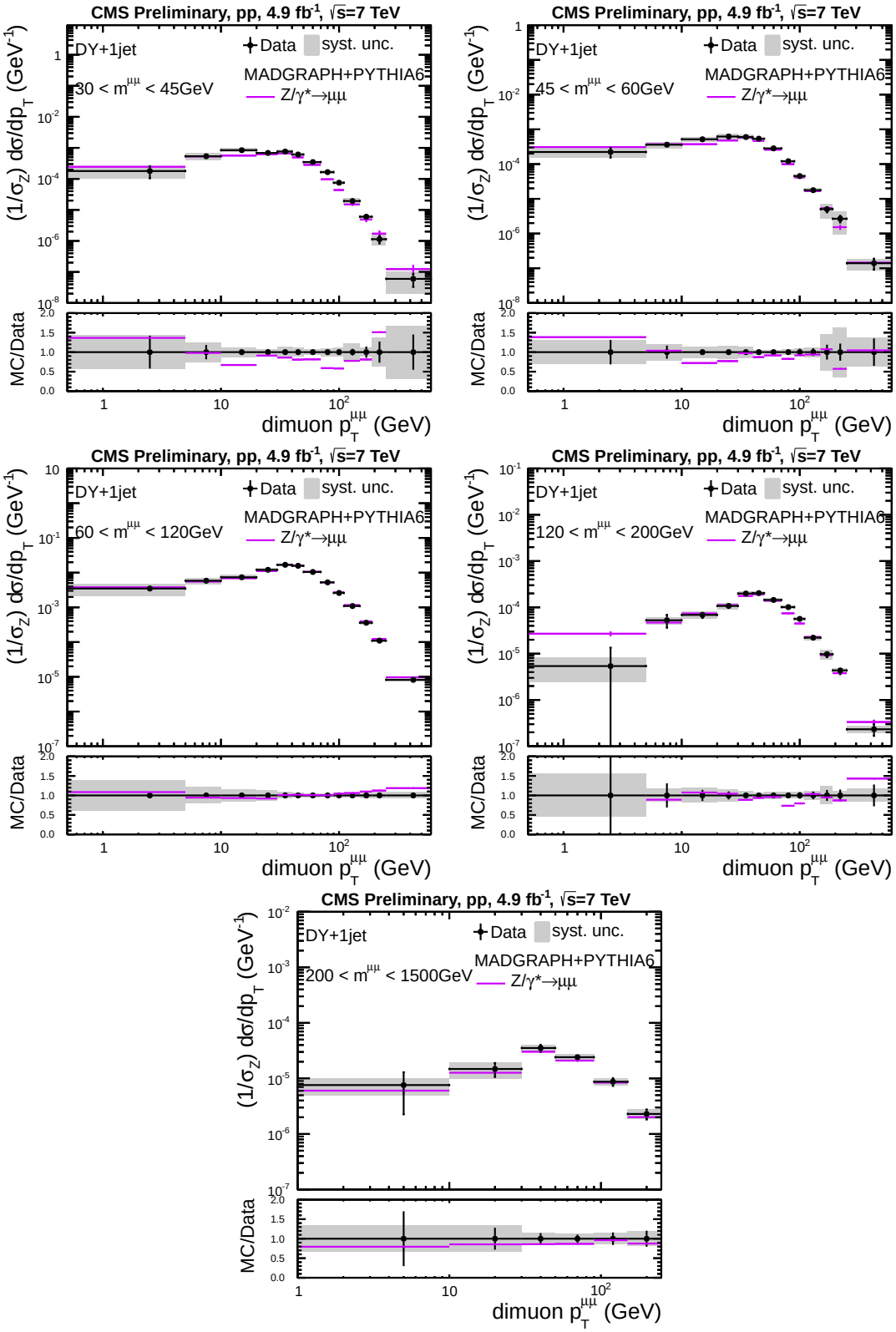

Figure 2: DY + 1 jet di-muon transverse momentum distribution normalized to the Z resonance region (60–120 GeV) in five different invariant mass regions covering the range from 30 – 1500 GeV. The vertical error bars on data indicate the statistical uncertainties and the error band represents the correlated systematic uncertainties. Data are compared to MADGRAPH + PYTHIA 6.

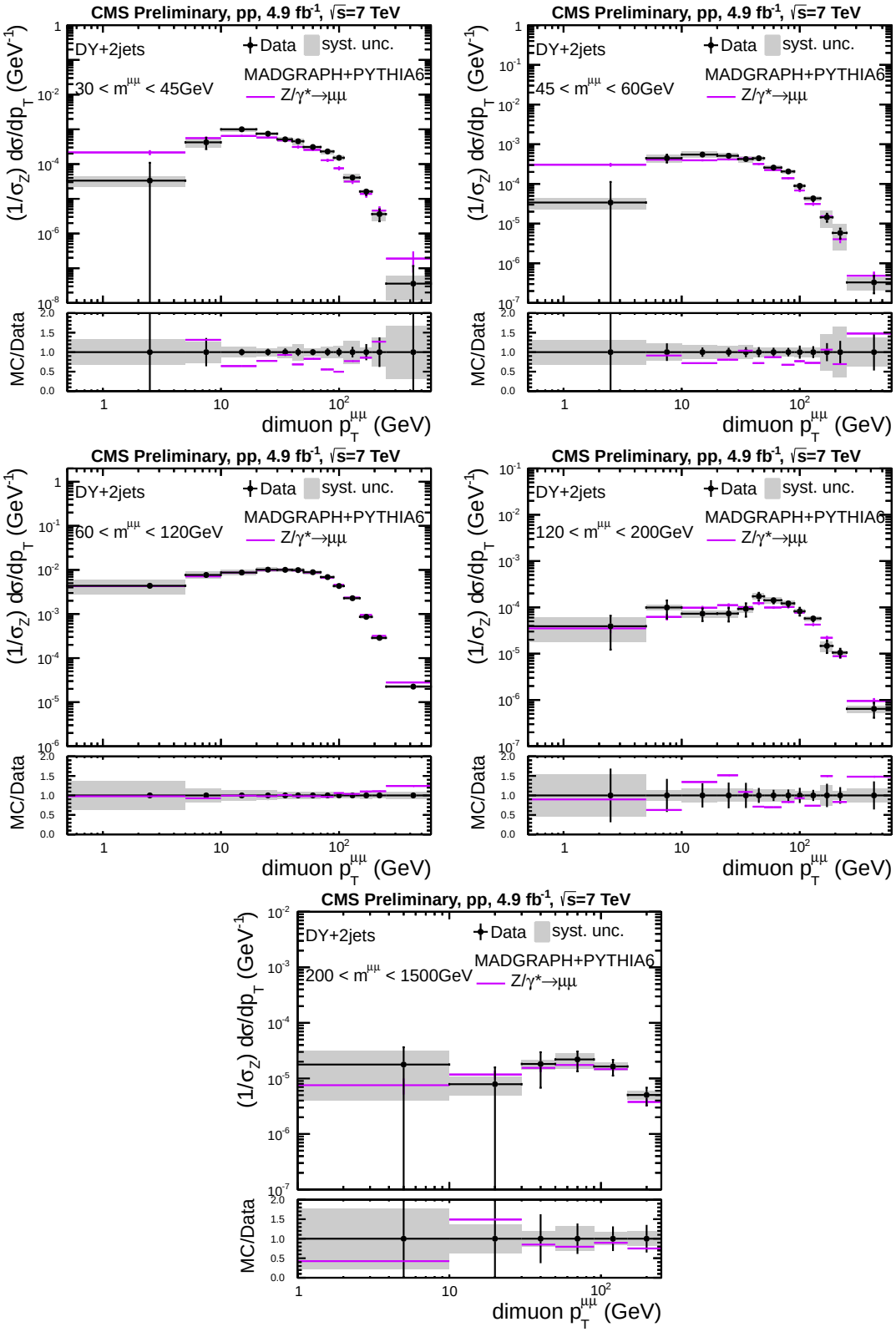

Figure 3: DY + 2 jets di-muon transverse momentum distribution normalized to the Z resonance region (60–120 GeV) in five different invariant mass regions covering the range from 30 – 1500 GeV. The vertical error bars on data indicate the statistical uncertainties and the error band represents the correlated systematic uncertainties. Data are compared to MADGRAPH + PYTHIA 6.

The double differential cross section for inclusive Drell-Yan production is shown for five different bins in the invariant mass $m^{\mu\mu}$ covering the range 30–1500 GeV. Overall a reasonable agreement between data and the predictions from MADGRAPH is observed. The results on the production of Drell-Yan in association with additional jets are presented in Fig. (2) and (3) for DY + 1 jet and DY + 2 jets respectively. The systematic uncertainties increase from the inclusive sample to DY + jets due to the JEC uncertainty.

The di-muon $p_{\mathrm{T}}^{\mu\mu}$ distribution for inclusive DY lepton pair production is rising from small $p_{\mathrm{T}}^{\mu\mu}$ towards a maximum at around 5 GeV and then falling towards large $p_{\mathrm{T}}^{\mu\mu}$. The distribution is well described by MADGRAPH. Discrepancies are observed for the low invariant mass bin 30–45 GeV for the inclusive DY production. A better agreement is expected when comparing to NNLO predictions [35]. The rising behavior at small $p_{\mathrm{T}}^{\mu\mu}$ is described by soft gluon resummation, and is treated in the simulation by initial state parton showers. A similar behavior is observed for the DY + 1 jet and DY + 2 jets distributions, however, the maximum is shifted to larger values, and in the case of DY + 1 jet the maximum is around 30 GeV, which is the p_{T} threshold for the jets. With the DY + 1 jet selection the range of soft gluon resummation is enlarged, from around 5 GeV in the inclusive case to around 30 GeV in the jet case, thus allowing to observe perturbative large p_{T} jet-resummation. In the simulation without initial state parton shower a sharp drop of the cross section below 30 GeV is observed (not shown here).

5.2 Drell-Yan Cross Section measurement as a function of the rapidity difference between the Drell-Yan pair and the leading jet

The double differential cross section $\frac{\mathrm{d}^2\sigma}{\mathrm{d}m\,\mathrm{d}|\Delta y(\mu\mu,\mathrm{j})|}$ is presented for the production of DY + 1 jet and DY + 2 jets. The cross section is measured in the three mass bins 30–60 GeV, 60–120 GeV and 120–1500 GeV. The Drell-Yan pair is required to fulfil $|\eta| > 2.5$. All cross sections are normalized to the Z boson mass region (60–120 GeV).

The normalized cross sections are presented in Fig. (4) for the production of DY + 1 jet and DY + 2 jets. MADGRAPH predicts a significantly different cross section as observed in the data, the distribution is shifted towards smaller rapidity differences. A similar trend is observed before correcting the data to stable particle level.

5.3 Jet multiplicity in Drell-Yan + jet events

The average jet multiplicity of jets with $p_{\mathrm{T}} > 30$ GeV between the leading jet and the forward Drell-Yan production as a function of the rapidity separation $\Delta y(\mu\mu, \mathrm{j})$ is presented in Fig. (5). Due to the limited number of recorded events the cross section is only shown in the Z boson mass range (60–120 GeV). The average jet multiplicity increases with increasing separation between the DY lepton pair and the leading jet from 0 to 0.3 at large rapidity separation. The general behavior is reproduced by the MADGRAPH simulation, however the increase in jet multiplicity in data is slower than what is predicted from the simulation.

6 Conclusion

The first measurement of the differential Drell-Yan and associated jets cross section as a function of the Drell-Yan di–muon mass is presented using an integrated luminosity of 4.9 fb^{-1}. The measurement is performed differentially as a function of the Drell-Yan pair transverse momentum for various di-muon mass ranges within 30–1500 GeV. The rapidity separation between the Drell-Yan muon pair and the leading jet is measured for different di–muon mass bins and the jet multiplicity as a function of Δy is presented for the Z mass region. The measured cross

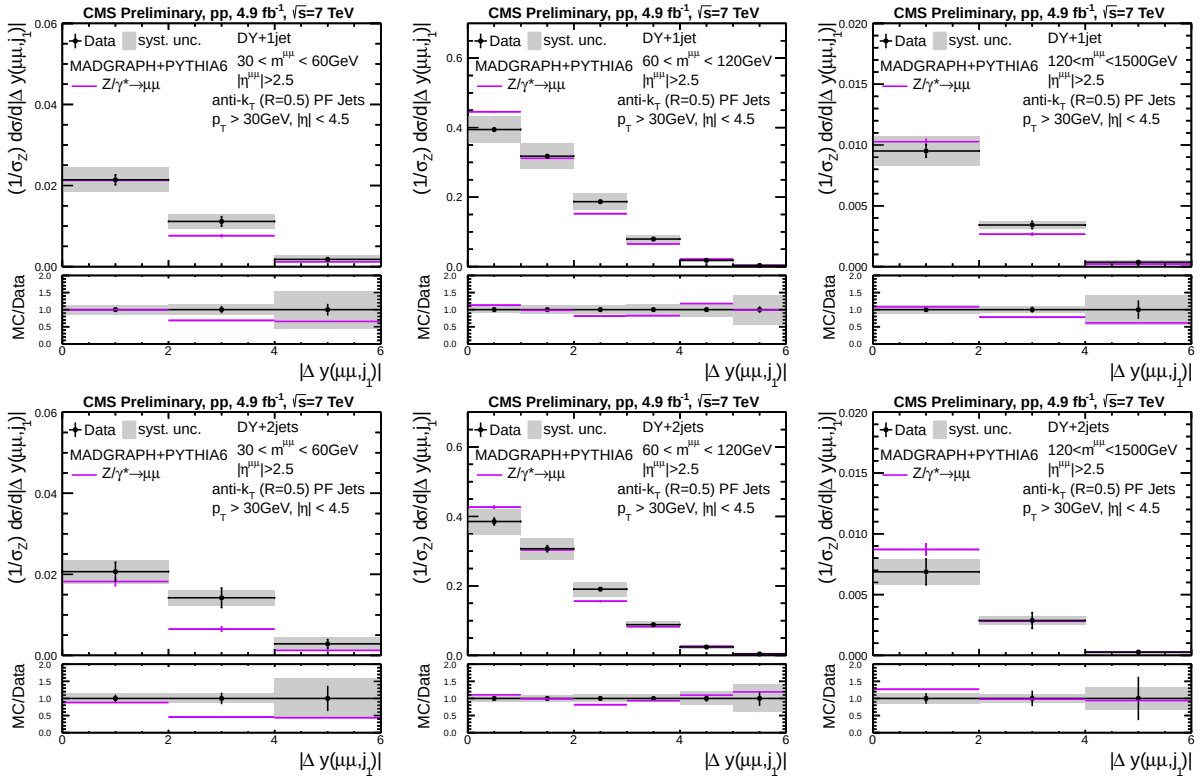

Figure 4: Drell-Yan di-muon rapidity difference between the Drell-Yan pair and the leading jet (normalized to the Z resonance region) for DY + 1 jet (upper row) and Drell-Yan + 2 jets (lower row) production. Data are compared to MADGRAPH + PYTHIA 6.

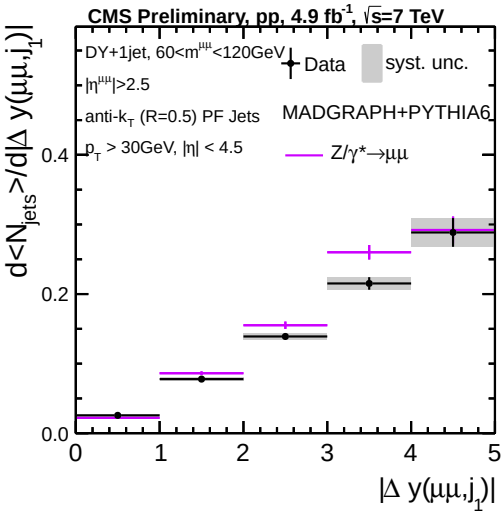

Figure 5: Average number of jets in forward Drell-Yan production as a function of the rapidity separation between the Drell-Yan di–muon and the leading jet. The measured cross section is compared to the MADGRAPH MC predictions.

sections are corrected to stable-particle level. The measured cross sections are compared to MADGRAPH $Z/\gamma^* \to \mu\mu$ predictions.

The measured p_{T} spectrum of DY lepton pair production is reasonably well described by the MADGRAPH simulation. The rise at small p_{T} in inclusive DY lepton pair production is a measure of soft gluon resummation, while the behavior at $p_{\mathrm{T}} < 30$ GeV in DY + jet production is a direct signal for perturbative jet resummation, which is well reproduced by initial state parton showers. The rapidity difference between DY lepton pair and the leading jet is not reproduced by the simulation and MADGRAPH predicts the jets to be closer to the DY lepton pair than observed in the data. The average jet multiplicity in the rapidity interval between the DY lepton pair and the leading jet is increasing with increasing separation, but the simulation predicts more jets.

References

[1] R. Hamberg, W. L. van Neerven, and T. Matsuura, "A complete calculation of the order α_s^2 correction to the Drell–Yan K-factor", *Nucl. Phys. B* **359** (1991) 343, doi:10.1016/0550-3213(91)90064-5.

[2] S. Catani et al., "Vector Boson Production at Hadron Colliders: A Fully Exclusive QCD Calculation at Next-to-Next-to-Leading Order ", *Phys. Rev. Lett.* **103** (2009) 082001, doi:10.1103/PhysRevLett.103.082001, arXiv:0903.2120.

[3] S. Catani and M. Grazzini, "Next-to-Next-to-Leading-Order Subtraction Formalism in Hadron Collisions and its Application to Higgs-Boson Production at the Large Hadron Collider ", *Phys. Rev. Lett.* **98** (2007) 222002, doi:10.1103/PhysRevLett.98.222002, arXiv:hep-ph/0703012.

[4] K. Melnikov and F. Petriello, "Electroweak gauge boson production at hadron colliders through $O(\alpha_s^2)$", *Phys. Rev. D* **74** (2006) 114017, doi:10.1103/PhysRevD.74.114017, arXiv:hep-ph/0609070.

[5] Y. L. Dokshitzer, D. Diakonov, and S. I. Troian, "On the Transverse Momentum Distribution of Massive Lepton Pairs", *Phys. Lett.* **B79** (1978) 269–272, doi:10.1016/0370-2693(78)90240-X.

[6] J. C. Collins, D. E. Soper, and G. F. Sterman, "Transverse Momentum Distribution in Drell-Yan Pair and W and Z Boson Production", *Nucl.Phys.* **B250** (1985) 199, doi:10.1016/0550-3213(85)90479-1.

[7] CMS Collaboration, "Measurement of the Rapidity and Transverse Momentum Distributions of Z Bosons in pp Collisions at $\sqrt{s} = 7$ TeV", *Phys.Rev.* **D85** (2012) 032002, doi:10.1103/PhysRevD.85.032002, arXiv:1110.4973.

[8] J. R. Andersen, V. Del Duca, F. Maltoni, and W. J. Stirling, "W boson production with associated jets at large rapidities", *JHEP* **05** (2001) 048, arXiv:hep-ph/0105146.

[9] P. Cipriano et al., "Higgs boson as a gluon trigger", *Phys. Rev. D* **88** (Nov, 2013) 097501, doi:10.1103/PhysRevD.88.097501.

[10] M. Cacciari and G. P. Salam, "Dispelling the N^3 myth for the k_t jet-finder", *Phys.Lett. B* **641** (2006) 57–61, doi:10.1016/j.physletb.2006.08.037, arXiv:hep-ph/0512210.

[11] M. Cacciari, G. P. Salam, and G. Soyez, "The anti-k_t jet clustering algorithm", *JHEP* **04** (2008) 063, doi:10.1088/1126-6708/2008/04/063, arXiv:0802.1189.

[12] M. Cacciari, G. P. Salam, and G. Soyez, "FastJet User Manual", *Eur.Phys.J. C* **72** (2012) 1896, doi:10.1140/epjc/s10052-012-1896-2, arXiv:1111.6097.

[13] CMS Collaboration, "Performance of CMS muon reconstruction in pp collision events at $\sqrt{s} = 7$ TeV", *JINST* **7** (2012) P10002, doi:10.1088/1748-0221/7/10/P10002, arXiv:1206.4071.

[14] CMS Collaboration, "Determination of the Jet Energy Scale in CMS with pp Collisions at $\sqrt{s} = 7$ TeV", *CMS Physics Analysis Summary* **CMS-PAS-JME-10-010** (2010).

[15] CMS Collaboration, "The CMS experiment at the CERN LHC", *JINST* **3** (2008) S08004, doi:10.1088/1748-0221/3/08/S08004.

[16] F. Maltoni and T. Stelzer, "MadEvent: Automatic event generation with MadGraph", *JHEP* **0302:027** (2003).

[17] T. Sjöstrand, S. Mrenna, and P. Skands, "PYTHIA 6.4 Physics and Manual", *JHEP* **0605:026** (2006).

[18] GEANT4 Collaboration, "GEANT4—a simulation toolkit", *Nucl. Instrum. Meth. A* **506** (2003) 250, doi:10.1016/S0168-9002(03)01368-8.

[19] C. Oleari, "The POWHEG-BOX", *Nucl. Phys. Proc. Suppl.* **205-206** (2010) 36, doi:10.1016/j.nuclphysbps.2010.08.016, arXiv:1007.3893.

[20] R. Field, "Early LHC Underlying Event Data-Findings and Surprises", (2010). arXiv:1010.3558v1.

[21] J. Pumplin et al., "New generation of parton distributions with uncertainties from global QCD analysis", *JHEP* **0207** (2002) 012, doi:10.1088/1126-6708/2002/07/012, arXiv:hep-ph/0201195.

[22] K. Rose, "Deterministic Annealing for Clustering, Compression, Classification, Regression, and Related Optimization Problems", in *Proceedings of the IEEE*, pp. 2210–2239. 1998.

[23] CMS Collaboration, "Particle–Flow Event Reconstruction in CMS and Performance for Jets, Taus, and $E_{\mathrm{T}}^{\mathrm{miss}}$", *CMS Physics Analysis Summary* **CMS-PAS-PFT-09-001** (2009).

[24] CMS Collaboration, "Commissioning of the Particle-Flow Reconstruction in Minimum-Bias and Jet Events from pp Collisions at 7 TeV", *CMS Physics Analysis Summary* **CMS-PAS-PFT-10-002** (2010).

[25] CMS Collaboration, "Pileup Jet Identification", *CMS Physics Analysis Summary* **CMS-PAS-JME-13-005** (2013).

[26] R. Kleiss and W. J. Stirling, "TOP QUARK PRODUCTION AT HADRON COLLIDERS: SOME USEFUL FORMULAE", *Z.Phys.* **C40** (1988) 419–423, doi:10.1007/BF01548856.

[27] U. Langenfeld, S. Moch, and P. Uwer, "Measuring the running top-quark mass", *Phys.Rev.* **D80** (2009) 054009, doi:10.1103/PhysRevD.80.054009, arXiv:0906.5273.

[28] CMS Collaboration, "Combination of top quark pair production cross section measurements", *CMS Physics Analysis Summary* **CMS-PAS-TOP-11-024** (2011).

[29] K. Melnikov and F. Petriello, "W Boson Production Cross Section at the Large Hadron Collider with $\mathcal{O}(\alpha_S^2)$ Corrections", *Phys. Rev. Lett.* **96** (Jun, 2006) 231803, doi:10.1103/PhysRevLett.96.231803.

[30] CMS Collaboration, "Measurements of Inclusive W and Z Cross Sections in pp Collisions at $\sqrt{s} = 7$ TeV", *JHEP* **1101** (2011) 080, doi:10.1007/JHEP01(2011)080, arXiv:1012.2466.

[31] G. D'Agostini, "A Multidimensional unfolding method based on Bayes theorem", *Nucl.Instrum.Meth.* **A362** (1995) 487.

[32] CMS Collaboration, "Determination of jet energy calibration and transverse momentum resolution in CMS", *J. Instrum.* **6** (2011) P11002, doi:10.1088/1748-0221/6/11/P11002.

[33] CMS Collaboration, "Jet Energy Resolution in CMS at $\sqrt{s} = 7$ TeV", *CMS Physics Analysis Summary* **CMS-PAS-JME-10-014** (2010).

[34] CMS Collaboration, "Measurement of the inelastic proton-proton cross section at $\sqrt{s} = 7$ TeV", *Phys. Lett. B* **722** (2013) 5, doi:10.1016/j.physletb.2013.03.024.

[35] CMS Collaboration, "Measurement of the differential and double-differential Drell-Yan cross sections in proton-proton collisions at $\sqrt{s} = 7$ TeV", *JHEP* **1312** (2013) 030, doi:10.1007/JHEP12(2013)030.